The effects of implant topography on osseointegration under estrogen deficiency induced osteoporotic conditions: histomorphometric, transcriptional and ultrastructural analysis.

Zhibin Du[a], Yin Xiao[a], Saeed Hashimi[b], Stephen M Hamlet[b], Saso Ivanovski[b*]

[a] Institute of Health and Biomedical Innovation, Queensland University of Technology, Kelvin Grove, Brisbane, Queensland, Australia

[b] School of Dentistry and Oral Health, Griffith University, Gold Coast Campus, Queensland, Australia

* Corresponding Author:

Prof Saso Ivanovski: Griffith University, Gold Coast Campus, Griffith Centre, G40_7.81, Parkland Drive, QLD 4222 Australia

Tel: +61756780741

Fax: +61756780708

Email: s.ivanovski@griffith.edu.au

Abstract

Compromised bone quality and or healing in osteoporosis are recognised risk factors for impaired dental implant osseointegration. This study examined the effects of 1) experimentally induced osteoporosis on titanium implant osseointegration and 2) the effect of modified implant surface topography on osseointegration under osteoporosis-like conditions. Machined and micro-roughened surface implants were placed into the maxillary first molar root socket of 64 ovariectomised and sham-operated Sprague-Dawley rats. Subsequent histological and SEM observations showed tissue maturation on the micro-rough surfaced implants in ovariectomised animals as early as 3 days post-implantation. The degree of osseointegration was also significantly higher around the micro-rough implants in ovariectomised animals after 14 days of healing although by day 28, similar levels of osseointegration were found for all test groups. The micro-rough implants significantly increased the early (day 3) gene expression of alkaline phosphatase, osteocalcin, receptor activator of nuclear factor kappa-B ligand and dentin matrix protein 1 in implant adherent cells. By day 7, the expression of inflammatory genes decreased while the expression of the osteogenic markers increased further although there were few statistically significant differences between the micro-rough and machined surfaces. Osteocyte morphology was also affected by estrogen deficiency with the size of the cells being reduced in trabecular bone. In conclusion, estrogen deficiency induced osteoporotic conditions negatively influenced the early osseointegration of machined implants while micro-rough implants compensated for these deleterious effects by enhancing osteogenic cell differentiation on the implant surface.

Statement of Significance

Lower bone density, poor bone quality and osseous microstructural changes are all features characteristic of osteoporosis likely to impair the osseointegration of dental implants. Using a clinically relevant trabecular bone model in the rat maxilla, we demonstrated histologically that the negative effects of surgically-induced osteoporosis on osseointegration could be ameliorated by the biomaterial's surface topography. Furthermore, gene expression analysis suggests this may be a result of enhanced osteogenic cell differentiation on the implant surface.

Key Words

Osteoporosis, rat, maxilla, dental implant, osseointegration, osteocyte.

1. **Introduction**

Osteoporosis is a chronic disease affecting over 200 million people worldwide [1]. Osteoporosis in the elderly, especially postmenopausal women is also significantly correlated with tooth loss [2-5]. Lower bone density, poor bone quality and osseous microstructural changes, all characteristics of osteoporosis, have been shown to delay the bone healing process of fractured bone [6-8]. Endosseous dental implant healing exhibits similar biological mechanisms to that observed in bone fracture healing [9-12], and hence may be influenced by osteoporotic conditions. The results of a recent systematic review show that osteoporotic patients have higher rates of dental implant loss [13]. Many animal studies have reported a lower rate of titanium implant osseointegration in osteoporotic environments, however the majority of these studies used long bone [14-18] rather than jaw bone models [19]. As there are significant differences in the embryological origin, ossification process and the response to osteoporotic conditions between long bones and craniofacial bones [20, 21], the relevance of results obtained in a long bone model to the oral environment is questionable. We have shown that the bone quality in the posterior rat maxilla is negatively affected by estrogen deficiency induced osteoporotic conditions [22], and that the first molar site in the posterior maxilla is a suitable model for dental implant research [23].

Early studies in the jawbone using an osteoporotic rat model showed no significant influence on osseointegration when using first-generation 'machined' implants [24-26]. However, contemporary implants have a 'micro-rough' implant topography which is known to influence peri-implant bone healing [27]. Indeed animal studies have shown that commercially available 'micro-rough' surfaced titanium implants result in superior bone to implant contact compared to 'smoother' machined surfaced implants [28, 29], as well as having superior torque removal values [30, 31]. Few studies have evaluated the influence of titanium implant surface topography on the early stages of bone healing during osseointegration under osteoporotic conditions [32, 33]. Furthermore, the underlying cellular and molecular mechanisms that may be influenced by surface topography during osseointegration under osteoporotic conditions are not well understood.

Therefore, in this study, the primary aim was to test the hypothesis that estrogen deficiency has a negative influence on implant healing which can be ameliorated by micro-rough implant surface topography. A secondary objective was to undertake ultrastructural and

gene expression analysis to elucidate the cellular and molecular mechanisms that may be influenced under these conditions.

2. Material and Methods

2.1. Animals

The Griffith University animal ethics committee approved the experimental protocol for the study (DOH/01/4/AEC). Sixty four three-month-old female Sprague-Dawley rats (Animal Resource Center,Western Australia) were used. This number of animals was chosen based on the results of histomorphometric analysis in similar studies using ovariectomised rats [15, 23]. Animals were fed standard rat chow and water ad libitum throughout the experiment. After acclimatization for 2 weeks, the rats were randomly divided into two groups, sham-operated (SHAM, n=32) and ovariectomised (OVX, n=32). Ovariectomy was performed according to our previously established methods [15, 22] where both histological and micro-CT analyses demonstrated successful induction of osteoporosis. SHAM group rats were also subjected to the same surgical procedure with an equivalent amount of fat tissue removed instead of the ovaries. All of the surgical procedures were performed under isoflurane (1–3%) inhalation anaesthesia. The animals were subsequently allowed to develop osteoporosis over three months prior to implant placement. This period of time has been shown to be sufficient to develop osteoporotic conditions in this model [22].

2.2. Implants

The surface roughness parameter 'Sa' (Arithmetic mean height) was analysed under 20×objective magnification using 3D optical microscopy (Contour Elite 3D, Bruker, US). 'minimally-rough' machined (Sa = 518.7±10.88nm; Sq = 643.4±30.53nm) and 'micro-rough' (Sa = 906.19±19.85nm; Sq = 1.11±0.09µm) surfaced titanium implants (2mm diameter x 3mm length) produced from Type IV commercially pure titanium were obtained from Southern Implants Ltd (Irene, South Africa). The micro-rough surfaced implant was prepared using the same techniques (aluminium oxide blasting) as used for commercially available dental implants [Fig.1].

2.3. Surgical Procedures

One implant of each surface type (machined and micro-rough) was placed bilaterally in the maxilla of all 64 animals 3 months after ovariectomy using a previously published protocol [23]. Briefly, implants were placed into the first molar mesial socket after tooth extraction. The osteotomy was prepared using a 1.2mm pilot drill and a 1.8mm diameter final drill (Southern Implants, Ltd., Irene, South Africa). All osteotomy procedures were

performed with copious saline irrigation. Machined and rough surfaced implants were placed into the prepared sockets with a torque of approximately 15Ncm until the implant shoulder was inserted to the level of the bone crest. The wound was then sutured with slowly resorbable sutures (5-0 Vicryl Ethicon, NJ, USA). Post-operative analgesia (buprenorphine 0.01 - 0.05mg/kg and carprofen 4 - 5mg/kg) and antibiotic cover (entrofloxacin 2.5mg/Kg) were administrated by intraperitoneal injection immediately after the surgery and continued daily for three days post-operatively.

To identify new bone formation the fluorescent dyes alizarin red S (25mg/kg, 3 days before sacrifice) and calcein (10mg/kg, 10 days prior to alizarin injection) were given intraperitoneally. Mineral apposition rate (MAR) is calculated as the distance between the midpoint of the corresponding edges of the two labels divided by the time between the labeling periods [34].

2.4. Sample Collection

Animals were sacrificed after 3, 7, 14 and 28 days of healing and samples were collected for histological, SEM and qPCR analysis. Five animals per group were used for the PCR analyses, while 2 animals per group were used for the histological and scanning electron microscopy observations at days 3 and 7, a total of 9 animals (18 implants) for each of the four test groups i.e SHAM and OVX; machined and micro-rough. For the longer-term healing histological and SEM observations at days 14 and 28, samples were collected from 7 animals (14 implants) per test group.

2.5. Histological Sample Preparation

Using a diamond-tipped circular saw, block sections of the maxilla containing the implants were collected and immediately fixed with 4% paraformaldehyde for 48h at 4°C. The samples were then dehydrated in a graded series of ethanol before being embedded in methylmetacrylate resin (Technovit® 7200 VLC, Heraeus Kulzer, Dormagen, Germany).

Thirty-micron thick sections of the maxilla containing the implant were prepared using a cutting and grinding system (EXAKT Apparatebau, Norderstedt, Germany) [35]. Two sections per implant were stained with methylene blue-alizarin red S and scanned using the Aperio ScanScope CS at 40 times magnification (Aperio Technologies Inc., Vista, CA).

Histomorphometric analysis was carried out using ImageScope™ software at 4 times magnification (Aperio Technologies Inc.) by a single blinded trained examiner.The

percentage of bone to implant contact (%BIC) was defined as the ratio of the sum of the implant length in direct contact with new bone tissue and the total length of the implant adjacent to native bone (each side contained at least two threads). New bone area (%BA) was defined as the percentage of mineralized bone tissue within the threaded areas of the implant that were adjacent to native bone [23].

2.6. Scanning electron microscopy

Samples (n=2 in each group) were fixed in 2.5% glutaraldehyde in 0.1 M sodium cacodylate buffer (PH 7.4) containing 0.05% tannic acid for at least 48h at 4ºC. The samples were then frozen in liquid nitrogen, followed by cryo-fracturing. At the early healing times (day3 and day7), as the implant has not fully integrated with bone the cryo-fracture technique is an effective method to allow separation of the dental implant from the bone [36]. SEM observation was carried using a field emission scanning electron microscope (Carl Zeiss Sigma VP Oxford Micro-analysis Field Emission Scanning Electron Microscopy, Germany).

For SEM analysis of osteocytes, polished resin embedded samples were first acid etched with 37% phosphoric acid for 10 seconds then immersed in 5% sodium hypochlorite for 5 min and air-dried overnight [22, 37]. The sections were subsequently coated with gold prior to SEM observation. This analysis was carried out only on the day 28 samples when osseointegration is complete and the relationship between osteocytes and the implant can be observed.

2.7. Quantitative RT-PCR

PCR was performed at days 3 and 7 to assess the early expression of genes associated with the healing microenvironment. After unscrewing the implant from the maxilla, tissue from the implant surface and socket wall was collected using a small dental curette and immediately immersed into TRIZOL reagent (Invitrogen). Total RNA was subsequently extracted from these samples according to the manufacturer's instructions. M-MuLV Reverse Transcriptase was then used to prepare complementary DNA (cDNA) according to the manufacture's protocols.

Oligonucleotide primers used to assess osteogenesis (alkaline phosphatase (ALP), osteocalcin (OC), alpha-1 type I collagen (COL1A)), osteoclast (receptor activator of nuclear factor kappa-B ligand (RANKL), tartrate-resistant acid phosphatase (TRAP)), osteocyte

(dentin matrix protein 1 (DMP1), sclerostin (SOST)) and inflammatory marker gene expression (tumor necrosis factor-alpha (TNFα), interleukin-1β (IL-1β)) are listed in table 1. Real-time PCR reactions (LightCycler 480 Real-Time PCR System, Roche, USA) were run using the following parameters: denaturation at 95˚C for 30 s and 40 cycles of amplification (95 ˚C for 10 s and 60 ˚C for 20 s). Quantification of gene expression was calculated using the delta Ct method and 90% PCR efficiency (k*1.9Δct) [38]. The expression of the targeted genes was normalised using the geometric average of three house-keeping genes (B2M, GAPDH and β-actin) [39].

2.8. Statistical analysis

As the data collected at the various time-point was from different animals i.e were not repeated measures, Two-way analysis of variance at each individual time point was used to assess the effect of the implant surface (machined vs. rough) and treatment group (SHAM vs. OVX) on %BIC, %BA, MAR and relative gene expression. One-way ANOVA at day 28 only was used to asses any difference in osteocyte body size. A p-value of <0.05 was considered significant.

3. Results

3.1 Histologic and SEM analysis of early healing at days 3and 7

All animals survived the surgical procedures and healing progressed uneventfully. After 3 days of healing, the cryo-fractured samples showed that more tissue was attached to the rough surfaced implants compared with the machined implants in both the SHAM and OVX groups [Fig. 2a, d; Fig. 3a, d]. At high magnification, the rough surfaced implants were seen to be covered by a layer of mixed tissue including matrix, fibres and cells (blood and inflammatory cells) [Fig. 2b; Fig. 3b]. However, on the machined implants, most of the surface was exposed or covered with a very thin mixed structure consisting of fibres and scattered cells with less amorphous matrix [Fig. 2e; Fig. 3e].

The morphology of the tissue covering both of the machined and micro-rough implant surfaces in the SHAM group revealed a denser consistency of fibres compared with the OVX group [Fig. 3b vs. Fig. 2b; Fig. 3e vs. Fig. 2e]. Red blood cells and adherent cells were visible on the surface of the implants in both the OVX and SHAM groups at this early stage of healing (Day 3).

Histological analysis revealed that the host bone was in contact with the implants in some areas, with fragments of old bone also sparsely distributed within the implant thread chambers. Osteoblasts were found to be present at this stage and were more obvious on the rough surfaced implants, especially in OVX animals, which showed osteoblasts regularly organized near the old bone surface [Fig. 2c]. A small amount of early osseointegration was observed on the micro-rough implants in the SHAM treated animals, with a thin layer of new bone seen to be forming directly on the implant surface [Fig.3c]. However, overall there was no obvious difference between the SHAM and OVX group for both micro-rough and machined implants at this early time-point [Fig. 2c, f; Fig. 3c, g].

Confocal fluorescence analysis at day 3 showed areas of new bone formation within the implant surgical site as shown by the uptake of calcein fluorescence by the new bone [Fig. 4]. Furthermore, the SHAM group were found to have more new bone formation than the OVX group, while micro-rough surfaced implants in the OVX group were associated with more new bone formation than machined implants [Fig. 4].

By day 7 of healing, under SEM observation, the micro-rough implants were again found to have more adherent tissue than the machined implants. The tissue attached to the implant

surfaces also seemed denser than it appeared at day 3 [Fig. 5a, d; Fig. 6a, e]. Under high magnification, fibers merged with each other to become thicker compared with their morphology at day 3 in both the SHAM and OVX groups. The fiber distribution in the SHAM group implants was thicker and more regular than the OVX group implants [Fig. 6b vs. Fig. 5b; Fig. 6f vs. Fig. 5e]. The rough surfaced implant group also showed more attached fibers than the machined implant group [Fig. 5b vs. 5e; Fig. 6b vs. 6f]. Osteoclast-like cells could be readily observed among the tissues associated with the OVX rough surfaced implants [Fig. 5b]. Red blood cells and adherent cells decreased compared with day 3 but still could be observed especially on the OVX machined implants [Fig. 5e].

Histology showed that new woven bone was formed around both machined and micro-rough surface implants. The SHAM group formed more bone to implant contact than the OVX group [Fig. 6c vs. Fig. 5c; Fig. 6g vs. Fig. 5f], and the micro-rough implant group showed more osseointegraton than the machined implant group [Fig. 5c vs. 5f; Fig. 6c vs. 6g]. The new bone formed in the SHAM micro-rough implant group [Fig 6c] appeared more mature (i.e. histological staining was more intense due to increased mineralisation) than the SHAM machine surface group where the less mineralised tissue stained lighter [Fig 6g], as well as both OVX groups [Fig. 5c,f]. New bone formation was also observed at the junction of the old bone surface in all groups. Both osteoblasts and osteoclasts could be observed, with osteoblasts arranged regularly along the new bone surface [Fig. 6d], and multinuclear osteoclasts located in the old bone surface within obvious bone resorption pits [Fig. 6h].

3.2. Gene expression

Two time points (day 3 and day 7) were selected for gene expression analysis of the early healing events. Gene markers were divided into four groups: osteogenesis (ALP, OC and COL-1A), osteoclast (RANKL and TRAP), osteocyte (DMP1 and SOST) and inflammation (TNFa and IL1b). At day 3 (Fig. 7), overall low levels of osteogenesis (ALP and OC), osteoclast (TRAP) and osteocyte (DMP1) gene expression was shown to be significantly higher on the SHAM micro-rough implants compared to the other groups. Osteoclast (RANKL) gene expression was also significantly increased in the OVX micro-rough implant group . Furthermore, expression of the osteocyte marker DMP1 was significantly increased in both the SHAM and OVX micro-rough implant groups when compared with the machined implant groups.

By day 7 (Fig. 8), the mean levels of gene expression of ALP, OC, COL-1A, RANKL, TRAP, DMP1 and SOST were increased in all groups from the day 3 levels. The osteoclast markers RANKL and TRAP were significantly increased in the SHAM micro-rough implant group compared with other groups. The osteocyte marker DMP1 was also significantly increased in the SHAM micro-rough group while SOST showed a trend towards increased levels at this timepoint. As expected with normal healing and the resolution of inflammation, the inflammation markers IL1b and TNFa at 7 days showed decreased expression compared to day 3.

3.3. Histomorphometric analysis of osseointegration at Days 14 and 28

Histological analysis was also performed on the day 14 and day 28 samples. At day 14, there was a significant amount of new bone around all implants for both the SHAM and OVX groups, with active osteoclasts and osteoblasts visible. The osteoblasts were arranged regularly around the new bone surface, while in some areas of the old bone, multinuclear osteoclasts could be observed in resorption pits (Fig. 9). There was no difference in %BIC between the SHAM micro-rough implant group (50.42 ± 2.25) and the SHAM machined implant group (52.95 ± 4.47). In addition, no difference in the %BIC was found between the SHAM micro-rough implant group and the OVX rough surfaced implant group (45.54 ± 4.33) (Fig. 10c, f). The OVX machined implant group (32.59 ± 2.24) had the least osseointegration as measured by %BIC, when compared with the OVX micro-rough implant group and SHAM machined implant group . However, there were no significant differences in %BA among the groups [Fig. 9, Fig. 10c, f].

At day 28, the new bone formed around the implants appeared to have a more mature and dense morphology than at day 14. The %BIC and %BA for all groups increased as expected with normal healing and no significant differences were observed between the groups at each time-point. Interestingly the %BIC in the OVX machined treatment group which was significantly lowere than the other treatment groups at day 14 had also increased to a similar level as that seen for the remaining groups by day 28 (Fig. 10c). Osteoblasts were still visible around the new bone surfaces however the number appeared fewer than at day 14. The mineralized apposition rate (MAR) as determined by fluorescence staining did not show any significant differences among the groups [Fig. 11].

3.4. Analysis of osteocytes.

Using the acid etching technique, SEM analysis of osteocytes in the trabecular bone showed that the cell bodies were morphologically smaller in the OVX than in the SHAM group, although the lacunae appeared similar (Fig. 12a,c; Fig. 13a,c d, e g). No difference in osteocytes were observed in cortical areas (Fig.13b, f, h). The osteocytes in the new bone areas (nearer to the implant) appear disorganized and smaller than the osteocytes in the old bone areas [Fig.12a, c]. Osteocytes in trabecular bone areas also show less uniformity than in the cortical areas where the osteocytes were arranged in a uniform parallel pattern with an elongated cell morphology [Fig. 13a, b, e, f]. The more distal from the new bone the more regular the osteocyte arrangement appeared. Osteocytes appeared to be in direct contact with the implant surface through dendrite like structures or indirectly through a thin layer of matrix which was in contact with the implant [Fig. 12b, d].

4. Discussion

The effect of osteoporosis on the osseointegration of titanium dental implants however continues to be a controversial issue [42, 43]. Osteoporosis has been shown to be a risk factor for implant failure [42] and it is unclear if this negative effect may be overcome by the use of implants with a micro-rough surface topography [44]. Examination of the extent to which surface modification can influence healing in a poor quality bone environment through the use of an osteoporotic animal model has important clinical implications, especially given the extensive incidence of osteoporosis in the general population.

Most osteoporotic animal models have utilized long bones, such as the tibia [15, 17, 18, 45, 46] or femur [16, 47] and the results from these studies is of limited value in understanding the osseointegration of endosseous implants into the jaw in osteoporotic conditions. Compared with long bone, the jaw bone has a different embryological origin and a different ossification mechanism, as well as a different response to estrogen deficiency [48, 49]. Thus, results from animal models of osteoporosis using the maxilla would be more comparable to dental implant osseointegration in osteoporotic patients. The results of this study show that both OVX and implant surface morphology affected the early healing events around titanium dental implants.

New bone formation was observed to be scattered in the implant thread chamber areas in the SHAM (micro-rough and machined) and OVX rough surface implant groups as identified by calcein uptake as early as day 3 post-implantation. New bone on the implant surface was also observed in the SHAM micro-rough surface implant at day 3. These findings are consistent with those reported by Schwarz et al (2007) showing bone formation as early as the 4th day post implant insertion [50]. It is noteworthy that these workers used a dog model rather than the rat which when compared with the dog, has a faster metabolism and hence accelerated healing [51]. The earliest histological evidence of bone-to-implant contact was seen on the SHAM micro-rough implants at Day 3, although this was only a sporadic finding and a limited sample size for histological analysis (n=2/group) at this timepoint. Nevertheless, if we consider the histological observations together with the cryo-facture analysis, which showed that the micro-rough surfaces had more attached tissue than the machined implants, it appears that the micro-rough implants were associated with accelerated tissue maturation and earlier surface bone formation compared to the machined implant. This is also consistent with previous findings that osseointegration occurs earlier on micro-rough surfaces via a process

of 'contact osteogenesis' directly on the implant, while only 'distance osteogenesis' originating from the borders of the surgically prepared recipient bone bed is observed with machined surfaces (Abrahamsson et al, 2004).

Previous studies in vitro have shown that surface topography can affect cellular recruitment [52] and promote osteoblast differentiation in vitro [53]. Micro-rough surface implants have been shown to increase osteoblastic cell attachment and differentiation [54-58] and result in higher osteogenic gene expression (ALP, bone sialoprotein, OC) compared with machined implants [59, 60]. Our study also found a significant increase in the expression of osteoblast markers (ALP and OC) in the SHAM micro-rough implant group, which is consistent with previously reported data [59] and provides further evidence that micro-rough surfaces have an enhanced osteogenic capacity compared to machined surfaces. However, the micro-rough implants in the OVX group did not show an increase in osteogenic gene expression despite an increase in the number and organization of osteoblasts shown histologically (compared to the OVX machined group). This may indicate that estrogen deficiency may interfere with the osteogenic capacity of osteoblasts during the early healing response.

Bone remodeling is a coordinated process triggered by osteoblast and osteoclast activity. Osteoclasts also play an important role in the initial period after implant placement [61, 62]. Osteoclast activation by micro-rough titanium surfaces in vitro has been shown to be similar to that of bone in vivo whereas activation is reduced by smooth titanium surfaces [63]. Furthermore, studies have shown that the gene expression of bone formation makers such as ALP, OC and collagen 1 is coupled with increased expression of osteoclast markers [64, 65]. Compared with the machined implants, our data showed that the SHAM micro-rough implant group not only significantly increased the expression of bone formation markers such as ALP and OC at day 3, but also significantly increased TRAP gene expression, which is consistent with these previous reports [64, 65]. Interestingly in the OVX micro-rough group, the gene expression of RANKL rather than TRAP significantly increased at day 3. The higher expression of RANKL could promote osteoclasts maturation, differentiation and activation through activation of the RANK\RANKL\OPG pathway [66, 67]. However, expression of bone formation markers did not increase, suggesting the estrogen deficiency may affect the balance between osteoblast and osteoclast activity in the early (day 3) healing process.

By day 7, inflammation marker gene expression was decreased as would be expected with the resolution of inflammation during healing [11] , while the gene expression of osteoblast, osteoclast and osteocyte markers was significantly elevated compared with day 3, which was consistent with previous reports [64, 68]. The increase in gene expression was also consistent with the histological and SEM observations, which showed more bone formation and more mature attached tissue around the implants.

Comparing groups at day 7, the SHAM micro-rough implants showed superior osteogenic capacity compared to the other groups, with increased gene expression of COL1A, RANKL and TRAP consistent with histological and SEM observations of increased bone formation and tissue maturation. OVX negatively influenced osteogenesis as COL1A expression in the OVX groups was found to be significantly lower than in the SHAM groups, which is consistent with previous clinical studies showing that high risk osteoporotic facture patients had lower levels of COL1A expression [54, 55]. The micro-rough implants showed some differences compared with the machined implants in the OVX group, with TRAP gene expression significantly increased. Although the TRAP expression was lower compared to the SHAM micro-rough implants at this time point, it reached a similar level of expression as SHAM machined implants. The results suggest that bone metabolism was enhanced around the micro-rough compared to the machined implants in the OVX group. The gene expression analysis was supported by both the SEM cryo-fracture and histologic assessment, which showed more mature tissue attached to the implant surface and more osseointegration formed around the micro-rough compared with machined implants. It is noteworthy that it is difficult to compare the %BIC between the different groups at the 7 day timepoint because the new bone formation is still very limited.

The role of osteocytes in the establishment of osseointegration was also assessed. Previous studies have shown that estrogen deficiency affects cancellous bone more than cortical bone [69, 70]. Our findings showed that ovariectomy significantly decreased the size of osteocytes in trabecular bone, while cortical bone was unaffected. The acid-etching protocol used to visualise osteocytes in this study removes mineralized tissue, leaving the non-mineralized and organic tissue intact. The larger lacunaes observed in the OVX group suggest that the lucanae contain a higher mineralised tissue content [71]. This finding is consitient with a recent study which showed that aged and osteoporotic conditions were characterised by an increase in the number and density of hypermineralized osteocyte lacunar [72]. These morphological changes could affect osteocyte function resulting in inferior

osseointegraton in the OVX groups during the early healing period. Furthermore, the increased expression of the osteocyte markers DMP1 and SOST suggests that the micro-rough surface triggers accelerated osteoblast differentiation to osteocytes. The advantages of the micro-rough implant were also supported by the SEM and histology observations.

By day 14, estrogen deficiency (OVX) negatively affected the osseointegration of the machined implants as indicated by a reduced %BIC compared with the SHAM group. Osseointegration of the micro-rough implants however was relatively unaffected with the %BIC similar to that seen in the SHAM group, suggesting that the micro-rough surface compensated for the negative effect of OVX.

By day 28, there were no significant differences among the groups in tersm of %BIC, %BA and mineral apposition rates (MAR), suggesting that the deleterious effects of machined surface topography or estrogen deficiency on osseointegration are diminished over time. Our results are consistent with a study which also compared three different surfaces (two different commercial rough surfaces c.f. a smooth surface implant) and showed significant differences only in the early healing time points (2 and 4 weeks), while there were no differences after 6 weeks [73]. The similarity in the degree of osseointegration between the OVX and SHAM groups at this late time-point (28 days) is also consistent with clinical reports which show no significant difference in long-term implant survival rates between osteoporosis and healthy subjects [45, 74, 75].

5. Conclusions

Both ovariectomy and implant morphology affected the early wound healing events associated with osseointegration. Estrogen deficiency delayed early bone healing around machined implants, while the micro-rough surface compensated for the negative effect(s) of ovariectomy by accelerating osseointegration via upregulation of the cellular and molecular osteogenic response.

References

[1] C. Cooper. Epidemiology of osteoporosis, Osteoporos Int. 9 Suppl 2 (1999) S2-8.
[2] P. Meisel, J. Reifenberger, R. Haase, M. Nauck, C. Bandt, T. Kocher. Women are periodontally healthier than men, but why don't they have more teeth than men?, Menopause (New York, NY). 15 (2008) 270-275.
[3] J. Darcey, K. Horner, T. Walsh, H. Southern, E.J. Marjanovic, H. Devlin. Tooth loss and osteoporosis: to assess the association between osteoporosis status and tooth number, British dental journal. 214 (2013) E10.
[4] J. Darcey, H. Devlin, D. Lai, T. Walsh, H. Southern, E. Marjanovic, K. Horner. An observational study to assess the association between osteoporosis and periodontal disease, British dental journal. 215 (2013) 617-621.
[5] K. Nicopoulou-Karayianni, P. Tzoutzoukos, A. Mitsea, A. Karayiannis, K. Tsiklakis, R. Jacobs, C. Lindh, P. van der Stelt, P. Allen, J. Graham, K. Horner, H. Devlin, S. Pavitt, J. Yuan. Tooth loss and osteoporosis: the OSTEODENT Study, Journal of clinical periodontology. 36 (2009) 190-197.
[6] V.S. Nikolaou, N. Efstathopoulos, G. Kontakis, N.K. Kanakaris, P.V. Giannoudis. The influence of osteoporosis in femoral fracture healing time, Injury. 40 (2009) 663-668.
[7] P. Giannoudis, C. Tzioupis, T. Almalki, R. Buckley. Fracture healing in osteoporotic fractures: is it really different? A basic science perspective, Injury. 38 Suppl 1 (2007) S90-99.
[8] U. Tarantino, I. Cerocchi, A. Scialdoni, L. Saturnino, M. Feola, M. Celi, F.M. Liuni, G. Iolascon, E. Gasbarra. Bone healing and osteoporosis, Aging Clin Exp Res. 23 (2011) 62-64.
[9] F. Marco, F. Milena, G. Gianluca, O. Vittoria. Peri-implant osteogenesis in health and osteoporosis, Micron. 36 (2005) 630-644.
[10] G.E. Salvi, D.D. Bosshardt, N.P. Lang, I. Abrahamsson, T. Berglundh, J. Lindhe, S. Ivanovski, N. Donos. Temporal sequence of hard and soft tissue healing around titanium dental implants, Periodontology 2000. 68 (2015) 135-152.
[11] S. Ivanovski, S. Hamlet, G.E. Salvi, G. Huynh-Ba, D.D. Bosshardt, N.P. Lang, N. Donos. Transcriptional profiling of osseointegration in humans, Clinical oral implants research. 22 (2011) 373-381.
[12] N. Donos, S. Hamlet, N.P. Lang, G.E. Salvi, G. Huynh-Ba, D.D. Bosshardt, S. Ivanovski. Gene expression profile of osseointegration of a hydrophilic compared with a hydrophobic microrough implant surface, Clinical oral implants research. 22 (2011) 365-372.
[13] G. Giro, L. Chambrone, A. Goldstein, J.A. Rodrigues, E. Zenobio, M. Feres, L.C. Figueiredo, A. Cassoni, J.A. Shibli. Impact of osteoporosis in dental implants: A systematic review, World journal of orthopedics. 6 (2015) 311-315.
[14] M. Chatterjee, K. Hatori, J. Duyck, K. Sasaki, I. Naert, K. Vandamme. High-frequency loading positively impacts titanium implant osseointegration in impaired bone, Osteoporos Int. (2014).
[15] Z. Du, J. Chen, F. Yan, Y. Xiao. Effects of Simvastatin on bone healing around titanium implants in osteoporotic rats, Clinical oral implants research. 20 (2009) 145-150.
[16] M. Fini, G. Giavaresi, P. Torricelli, A. Krajewski, A. Ravaglioli, M.M. Belmonte, G. Biagini, R. Giardino. Biocompatibility and osseointegration in osteoporotic bone, J Bone Joint Surg Br. 83 (2001) 139-143.
[17] J. Dudeck, S. Rehberg, R. Bernhardt, W. Schneiders, O. Zierau, M. Inderchand, J. Goebbels, G. Vollmer, P. Fratzl, D. Scharnweber, S. Rammelt. Increased bone remodelling around titanium implants coated with chondroitin sulfate in ovariectomized rats, Acta Biomater. 10 (2014) 2855-2865.
[18] B. Chen, Y. Li, X. Yang, H. Xu, D. Xie. Zoledronic acid enhances bone-implant osseointegration more than alendronate and strontium ranelate in ovariectomized rats, Osteoporos Int. 24 (2013) 2115-2121.

[19] Y.E. Viera-Negron, W.H. Ruan, J.N. Winger, X. Hou, M.M. Sharawy, J.L. Borke. Effect of ovariectomy and alendronate on implant osseointegration in rat maxillary bone, The Journal of oral implantology. 34 (2008) 76-82.
[20] B.R. Olsen, A.M. Reginato, W. Wang. Bone development, Annual review of cell and developmental biology. 16 (2000) 191-220.
[21] J.A. Helms, R.A. Schneider. Cranial skeletal biology, Nature. 423 (2003) 326-331.
[22] Z. Du, R. Steck, N. Doan, M.A. Woodruff, S. Ivanovski, Y. Xiao. Estrogen Deficiency-Associated Bone Loss in the Maxilla: A Methodology to Quantify the Changes in the Maxillary Intra-radicular Alveolar Bone in an Ovariectomized Rat Osteoporosis Model, Tissue engineering Part C, Methods. 21 (2015) 458-466.
[23] Z. Du, R.S. Lee, S. Hamlet, N. Doan, S. Ivanovski, Y. Xiao. Evaluation of the first maxillary molar post-extraction socket as a model for dental implant osseointegration research, Clinical oral implants research. (2015) doi: 10.1111/clr.12571. [Epub ahead of print].
[24] M. Nasu, Y. Amano, A. Kurita, T. Yosue. Osseointegration in implant-embedded mandible in rats fed calcium-deficient diet: a radiological study, Oral Dis. 4 (1998) 84-89.
[25] T. Fujimoto, A. Niimi, T. Sawai, M. Ueda. Effects of steroid-induced osteoporosis on osseointegration of titanium implants, Int J Oral Maxillofac Implants. 13 (1998) 183-189.
[26] G. Giro, P.G. Coelho, R. Sales-Pessoa, R.M. Pereira, T. Kawai, S.R. Orrico. Influence of estrogen deficiency on bone around osseointegrated dental implants: an experimental study in the rat jaw model, Journal of oral and maxillofacial surgery : official journal of the American Association of Oral and Maxillofacial Surgeons. 69 (2011) 1911-1918.
[27] R.M. Pilliar. Implant surface design for development and maintenance of osseointegration, Bio-implant Interface Improving Material and Tissue Reaction CRC press, Boca Raton, pp. (2003) 43-58.
[28] D. Buser, R.K. Schenk, S. Steinemann, J.P. Fiorellini, C.H. Fox, H. Stich. Influence of surface characteristics on bone integration of titanium implants. A histomorphometric study in miniature pigs, J Biomed Mater Res. 25 (1991) 889-902.
[29] D.L. Cochran, R.K. Schenk, A. Lussi, F.L. Higginbottom, D. Buser. Bone response to unloaded and loaded titanium implants with a sandblasted and acid-etched surface: a histometric study in the canine mandible, J Biomed Mater Res. 40 (1998) 1-11.
[30] D. Buser, T. Nydegger, H.P. Hirt, D.L. Cochran, L.P. Nolte. Removal torque values of titanium implants in the maxilla of miniature pigs, Int J Oral Maxillofac Implants. 13 (1998) 611-619.
[31] D. Buser, T. Nydegger, T. Oxland, D.L. Cochran, R.K. Schenk, H.P. Hirt, D. Snetivy, L.P. Nolte. Interface shear strength of titanium implants with a sandblasted and acid-etched surface: a biomechanical study in the maxilla of miniature pigs, J Biomed Mater Res. 45 (1999) 75-83.
[32] H.S. Alghamdi, J.A. Jansen. Bone regeneration associated with nontherapeutic and therapeutic surface coatings for dental implants in osteoporosis, Tissue engineering Part B, Reviews. 19 (2013) 233-253.
[33] N. Mardas, F. Schwarz, A. Petrie, A.R. Hakimi, N. Donos. The effect of SLActive surface in guided bone formation in osteoporotic-like conditions, Clinical oral implants research. 22 (2011) 406-415.
[34] D.W. Dempster, J.E. Compston, M.K. Drezner, F.H. Glorieux, J.A. Kanis, H. Malluche, P.J. Meunier, S.M. Ott, R.R. Recker, A.M. Parfitt. Standardized nomenclature, symbols, and units for bone histomorphometry: a 2012 update of the report of the ASBMR Histomorphometry Nomenclature Committee, Journal of bone and mineral research : the official journal of the American Society for Bone and Mineral Research. 28 (2013) 2-17.
[35] K. Donath, G. Breuner. A method for the study of undecalcified bones and teeth with attached soft tissues*, Journal of Oral Pathology & Medicine. 11 (1982) 318-326.
[36] D.E. Steflik, A.L. Sisk, G.R. Parr, P.J. Hanes, F. Lake, M.J. Song, P. Brewer, R.V. McKinney. High-voltage electron microscopy and conventional transmission electron microscopy of the interface zone between bone and endosteal dental implants, J Biomed Mater Res. 26 (1992) 529-545.

[37] J.Q. Feng, L.M. Ward, S. Liu, Y. Lu, Y. Xie, B. Yuan, X. Yu, F. Rauch, S.I. Davis, S. Zhang, H. Rios, M.K. Drezner, L.D. Quarles, L.F. Bonewald, K.E. White. Loss of DMP1 causes rickets and osteomalacia and identifies a role for osteocytes in mineral metabolism, Nature genetics. 38 (2006) 1310-1315.
[38] M.W. Pfaffl. A new mathematical model for relative quantification in real-time RT-PCR, Nucleic acids research. 29 (2001) e45.
[39] J. Vandesompele, K. De Preter, F. Pattyn, B. Poppe, N. Van Roy, A. De Paepe, F. Speleman. Accurate normalization of real-time quantitative RT-PCR data by geometric averaging of multiple internal control genes, Genome biology. 3 (2002) RESEARCH0034.
[40] L.W. Lindquist, G.E. Carlsson, T. Jemt. A prospective 15-year follow-up study of mandibular fixed prostheses supported by osseointegrated implants. Clinical results and marginal bone loss, Clinical oral implants research. 7 (1996) 329-336.
[41] Lambert FE, Weber HP, Susarla SM, Belser UC, Gallucci GO. Descriptive analysis of implant and prosthodontic survival rates with fixed implant-supported rehabilitations in the edentulous maxilla. J Periodontol. 80 (2009) 1220-30.
[42] G. Alsaadi, M. Quirynen, A. Komarek, D. van Steenberghe. Impact of local and systemic factors on the incidence of oral implant failures, up to abutment connection, Journal of clinical periodontology. 34 (2007) 610-617.
[43] E. Dervis. Oral implications of osteoporosis, Oral Surg Oral Med Oral Pathol Oral Radiol Endod. 100 (2005) 349-356.
[44] G. Alsaadi, M. Quirynen, K. Michiles, W. Teughels, A. Komarek, D. van Steenberghe. Impact of local and systemic factors on the incidence of failures up to abutment connection with modified surface oral implants, Journal of clinical periodontology. 35 (2008) 51-57.
[45] M.M. Bornstein, N. Cionca, A. Mombelli. Systemic conditions and treatments as risks for implant therapy, Int J Oral Maxillofac Implants. 24 Suppl (2009) 12-27.
[46] L. Maimoun, T.C. Brennan, I. Badoud, V. Dubois-Ferriere, R. Rizzoli, P. Ammann. Strontium ranelate improves implant osseointegration, Bone. 46 (2010) 1436-1441.
[47] H.S. Alghamdi, V.M. Cuijpers, J.G. Wolke, J.J. van den Beucken, J.A. Jansen. Calcium-phosphate-coated oral implants promote osseointegration in osteoporosis, J Dent Res. 92 (2013) 982-988.
[48] H.R. Dominguez-Malagon, E. Gonzalez-Conde, A.M. Cano-Valdez, K. Luna-Ortiz, A. Mosqueda-Taylor. Expression of hormonal receptors in osteosarcomas of the jaw bones: clinico-pathological analysis of 21 cases, Med Oral Patol Oral Cir Bucal. 19 (2014) e44-48.
[49] Y. Chai, R.E. Maxson, Jr. Recent advances in craniofacial morphogenesis, Developmental dynamics : an official publication of the American Association of Anatomists. 235 (2006) 2353-2375.
[50] F. Schwarz, D. Ferrari, M. Herten, I. Mihatovic, M. Wieland, M. Sager, J. Becker. Effects of surface hydrophilicity and microtopography on early stages of soft and hard tissue integration at non-submerged titanium implants: an immunohistochemical study in dogs, Journal of periodontology. 78 (2007) 2171-2184.
[51] J.P. Schmitz, J.O. Hollinger. The critical size defect as an experimental model for craniomandibulofacial nonunions, Clinical orthopaedics and related research. (1986) 299-308.
[52] C.R. Howlett, M.D. Evans, W.R. Walsh, G. Johnson, J.G. Steele. Mechanism of initial attachment of cells derived from human bone to commonly used prosthetic materials during cell culture, Biomaterials. 15 (1994) 213-222.
[53] Z. Schwartz, C.H. Lohmann, J. Oefinger, L.F. Bonewald, D.D. Dean, B.D. Boyan. Implant surface characteristics modulate differentiation behavior of cells in the osteoblastic lineage, Advances in dental research. 13 (1999) 38-48.
[54] T.P. Kunzler, T. Drobek, M. Schuler, N.D. Spencer. Systematic study of osteoblast and fibroblast response to roughness by means of surface-morphology gradients, Biomaterials. 28 (2007) 2175-2182.
[55] M. Herrero-Climent, P. Lazaro, J. Vicente Rios, S. Lluch, M. Marques, J. Guillem-Marti, F.J. Gil. Influence of acid-etching after grit-blasted on osseointegration of titanium dental implants: in vitro and in vivo studies, Journal of materials science Materials in medicine. 24 (2013) 2047-2055.

[56] J. Lincks, B.D. Boyan, C.R. Blanchard, C.H. Lohmann, Y. Liu, D.L. Cochran, D.D. Dean, Z. Schwartz. Response of MG63 osteoblast-like cells to titanium and titanium alloy is dependent on surface roughness and composition, Biomaterials. 19 (1998) 2219-2232.
[57] B.D. Boyan, L.F. Bonewald, E.P. Paschalis, C.H. Lohmann, J. Rosser, D.L. Cochran, D.D. Dean, Z. Schwartz, A.L. Boskey. Osteoblast-mediated mineral deposition in culture is dependent on surface microtopography, Calcified tissue international. 71 (2002) 519-529.
[58] P. O'Hare, B.J. Meenan, G.A. Burke, G. Byrne, D. Dowling, J.A. Hunt. Biological responses to hydroxyapatite surfaces deposited via a co-incident microblasting technique, Biomaterials. 31 (2010) 515-522.
[59] T. Hara, K. Matsuoka, K. Matsuzaka, M. Yoshinari, T. Inoue. Effect of surface roughness of titanium dental implant placed under periosteum on gene expression of bone morphogenic markers in rat, Bull Tokyo Dent Coll. 53 (2012) 45-50.
[60] N. Donos, M. Retzepi, I. Wall, S. Hamlet, S. Ivanovski. In vivo gene expression profile of guided bone regeneration associated with a microrough titanium surface, Clinical oral implants research. 22 (2011) 390-398.
[61] M. Marchisio, M. Di Carmine, R. Pagone, A. Piattelli, S. Miscia. Implant surface roughness influences osteoclast proliferation and differentiation, J Biomed Mater Res B Appl Biomater. 75 (2005) 251-256.
[62] C. Minkin, V.C. Marinho. Role of the osteoclast at the bone-implant interface, Advances in dental research. 13 (1999) 49-56.
[63] J. Brinkmann, T. Hefti, F. Schlottig, N.D. Spencer, H. Hall. Response of osteoclasts to titanium surfaces with increasing surface roughness: an in vitro study, Biointerphases. 7 (2012) 34.
[64] O. Omar, S. Svensson, N. Zoric, M. Lenneras, F. Suska, S. Wigren, J. Hall, U. Nannmark, P. Thomsen. In vivo gene expression in response to anodically oxidized versus machined titanium implants, Journal of biomedical materials research Part A. 92 (2010) 1552-1566.
[65] M. Monjo, S.F. Lamolle, S.P. Lyngstadaas, H.J. Ronold, J.E. Ellingsen. In vivo expression of osteogenic markers and bone mineral density at the surface of fluoride-modified titanium implants, Biomaterials. 29 (2008) 3771-3780.
[66] L.C. Hofbauer, S. Khosla, C.R. Dunstan, D.L. Lacey, W.J. Boyle, B.L. Riggs. The roles of osteoprotegerin and osteoprotegerin ligand in the paracrine regulation of bone resorption, Journal of bone and mineral research : the official journal of the American Society for Bone and Mineral Research. 15 (2000) 2-12.
[67] W.C. Dougall. Molecular pathways: osteoclast-dependent and osteoclast-independent roles of the RANKL/RANK/OPG pathway in tumorigenesis and metastasis, Clinical cancer research : an official journal of the American Association for Cancer Research. 18 (2012) 326-335.
[68] S. Ivanovski, S. Hamlet, M. Retzepi, I. Wall, N. Donos. Transcriptional profiling of "guided bone regeneration" in a critical-size calvarial defect, Clinical oral implants research. 22 (2011) 382-389.
[69] R.T. Turner, J.J. Vandersteenhoven, N.H. Bell. The effects of ovariectomy and 17 beta-estradiol on cortical bone histomorphometry in growing rats, Journal of bone and mineral research : the official journal of the American Society for Bone and Mineral Research. 2 (1987) 115-122.
[70] T.J. Wronski, C.C. Walsh, L.A. Ignaszewski. Histologic evidence for osteopenia and increased bone turnover in ovariectomized rats, Bone. 7 (1986) 119-123.
[71] Z. Du, S. Ivanovski, S.M. Hamlet, J.Q. Feng, Y. Xiao. The Ultrastructural Relationship Between Osteocytes and Dental Implants Following Osseointegration, Clinical implant dentistry and related research. 18 (2016) 270-280.
[72] V.T. Carpentier, J. Wong, Y. Yeap, C. Gan, P. Sutton-Smith, A. Badiei, N.L. Fazzalari, J.S. Kuliwaba. Increased proportion of hypermineralized osteocyte lacunae in osteoporotic and osteoarthritic human trabecular bone: implications for bone remodeling, Bone. 50 (2012) 688-694.
[73] M. Adam, C. Ganz, W.G. Xu, H.R. Sarajian, B. Frerich, T. Gerber. How to Enhance Osseointegration–Roughness, Hydrophilicity or Bioactive Coating, Key Engineering Materials. 493 (2012) 467-472.

[74] A. Mellado-Valero, J.C. Ferrer-Garcia, J. Calvo-Catala, C. Labaig-Rueda. Implant treatment in patients with osteoporosis, Med Oral Patol Oral Cir Bucal. 15 (2010) e52-57.
[75] B. Friberg, A. Ekestubbe, D. Mellstrom, L. Sennerby. Branemark implants and osteoporosis: a clinical exploratory study, Clinical implant dentistry and related research. 3 (2001) 50-56.

Fig.1. Machined (a, b) and micro-rough (b, c) surfaced implants viewed under SEM. The roughness (Sa) of the implants in both implant thread valley and apex areas (red rectangles) as measured by 3D optical microscopy were 518.7±15.38 nm for the machined surface implant (d) and 906.19±28.07 nm for the micro-rough surfaced implant (e).

Fig.2. Cryo-fracture SEM and histology images of implants after 3 days of healing in the OVX group. The micro-rough surfaced implant showed more adherent mixed tissue compared to the machined implant (a, b vs. d, e), the attached mixed tissue include fibres, cells and amorphous matrix (b). The machined implant was covered with a thinner layer of tissue with clear fibres and cells (e). Histological analysis showed the micro-rough surfaced implant had osteoblasts organised near the old bone surface (c, yellow arrows) compared with the machined surface (f).

Fig.3. Cryo-fracture SEM and histology images of implants after 3 days of healing in the SHAM group. The micro-rough surfaced implant again had more adherent tissue than the machined surface (a, b vs. d, e), which is consistent with the OVX results (Fig. 2). However, the tissue's quality, especially the fibres in the SHAM group appears to be better than the OVX group (Fig. 3b vs. Fig. 2b; Fig. 3e vs. Fig. 2e). Inflammatory cells are easily visible at this stage (e, purple arrow). Histological images show the earliest osseointegration was seen in the SHAM micro-rough surface implant (d, orange arrow).

Fig.4. Calcein and Alizarin red staining of day 3 new bone formation. Confocal imaging revealed new bone formation in SHAM group implants (a, b) and OVX rough (c) surface implant (green fluorescence). However, compared with the SHAM group, new bone formed in the OVX group is limited, which indicates early osteogenesis could be inhibited by ovariectomy. OVX machined (d) surface implants showed almost no new bone formation at this stage.

Fig.5. Cryo-fracture SEM and histology images at day 7 in OVX group. Micro-rough surface implants (a, b) continued to attach more tissue than the machined surface implant (d, e). The attached tissue became more compact and the fibres merged with each other at this stage compared with day 3 results (Fig. 2). OVX rough surface implant attached more tissue than machined surface implant, with more osteoclast-like cells attached on the implant surface (b,

green arrow); relative more blood and inflammatory cells can still been seen in the machined surface implant (e, purple arrow). Histology images showed the rough surface implant (c) with more osseointegration than machined surface implant (f), both ostoblasts and osteoclasts are visible.

Fig.6. Cryo-fracture SEM and histology images of day 7 results in the SHAM group. More tissue was attached to the micro-rough surface than the machined surface implant. SHAM rough surface showed attached regular merged fibres, with less mixed cells than machined surface implant (Fig. a, b vs. e, f). The SHAM group attached tissue clearly showed better quality than OVX group (Fig. 6b vs. Fig.5b; Fig. 6f vs. Fig. 5e). Histology images showed the SHAM rough surface implant not only has more osseointegration than machined surface implant, but also has the most mature bone compared with SHAM machined implant (g) and OVX group implants (Fig. 5c, f). Both osteoblasts (d) and osteoclasts (h) are visible. Yellow arrows show the new bone quality, orange arrows show the osteoblasts and green arrows show the osteoclasts).

Fig.7. Day 3 gene expression analysis of early bone and inflammatory markers. ALP, OC, DMP1 and TRAP were significantly increased in the SHAM rough surface implant while RANKL and DMP1 were significantly increased in the OVX rough surface implants compared to the machined implants (*$p<0.05$, **$p<0.01$).

Fig.8. Day 7 COL1A and DMP1 gene expression for both machined and micro-rough implants was significantly increased in the SHAM compared to OVX group. SHAM rough surface implants showed significant increases in RANKL and TRAP gene expression compared with other groups (*$p<0.05$, **$p<0.01$).

Fig.9. Histology results at day 14. New bone was formed around the implant in all groups. SHAM group implant and OVX rough surface implant showed more osseintegration than the OVX machined surface implant (Fig.9c). Both osteoblasts (yellow arrows) and ostoeclasts (green arrows) are active at this stage. However, the OVX machined surface implant shows more osteoclasts.

Fig.10. Histology results at day 28. The new bone appears more mature than at day 14 (Fig. 9). Active osteoblasts can still be seen on the new bone surface however ostoeclast numbers appear to be lower compared with the day 14 results. While %BIC was significantly lower in the OVX machined group at day 14, the effect of OVX was not apparent in the rough group which was similar to that seen for the SHAM groups. By day 28, there were few significant differences in either %BIC or BA between all the groups (c, f) (*$p<0.05$).

Fig.11. Calcein and Alizarin red staining of new bone formation at day 28 (a,b). There was no difference in the mineralized apposition rate (MAR) between groups (c).

Fig.12. SEM images of acid-etched resin-embedded samples showing osteocytes around implant. Similar images were obtained at all healing time-points. The newly formed osteocytes are smaller, round, less polar, and disorganized than the osteocytes in the old bone areas (a, c,). Osteocytes are in direct contact (circle) or indirect contact (rectangle) with the implant (b, d).

Fig.13. The osteocyte's body (yellow dotted circle) within the lacunae (green dotted circle) in the SHAM group (a, c) are larger than the OVX group (e, g) in trabecular bone area (d), however, there was no difference between cortical areas (b, f, h). (Blue arrows indicate the osteocyte/lacunae morphology).

Primer Sequences Used for Real-time PCR	
Genes	**Primers (F = forward; R = reverse)**
B2M	F: 5'-CGAGACCGATGTATATGCTTGC-3'
	R: 5'-GTCCAGATGATTCAGAGCTCCA-3'
GAPDH	F: 5'-CAAGTTCAACGGCACAGTCAAG-3'
	R: 5'-ACATACTCAGCACCAGCATCAC-3'
β-actin	F: 5'-CACCCGCGAGTACAACCTTC-3'
	R: 5'-CCCATACCCACCATCACACC-3'
ALP	F: 5'-TCGGACAATGAGATGCGCC-3'
	R: 5'-TGGGAGTGCTTGTGTCTAGG-3'
OC	F: 5'-GCCCTGACTGCATTCTGCCTCT-3'
	R: 5'-TCACCACCTTACTGCCCTCCTG-3'
COL1A	F: 5'-GGAGAGAGCATGACCGATGG-3'
	R: 5'-GAATCGACTGTTGCCTTCGC-3'
RANKL	F: 5'-CATGAAACCTCAGGGAGCGT-3'
	R: 5'-GTTGGACACCTGGACGCTAA-3'
TRAP	F: 5'-CAGCCCTTATTACCGTTTGC-3'
	R: 5'-GAATTGCCACACAGCATCAC-3'
DMP1	F: 5'-CTTTTGACCCAGTCGGAAGAGA-3'
	R: 5'-CTATTTGCCATGGGCGGTGG-3'
SOST	F: 5'-CCTTCAAGAATGATGCCACA-3'
	R: 5'-ACTCGGACACGTCTTTGGTG-3'
TNFa	F: 5'-TACTGAACTTCGGGGTGATCG-3'
	R: 5'-CCTTGTCCCTTGAAGAGAACC-3'
IL1b	F: 5'-AGCTTCAGGAAGGCAGTGTC-3'
	R: 5'-TCAGACAGCACGAGGCATTT-3'

Table 1. RTPCR primer sequences.

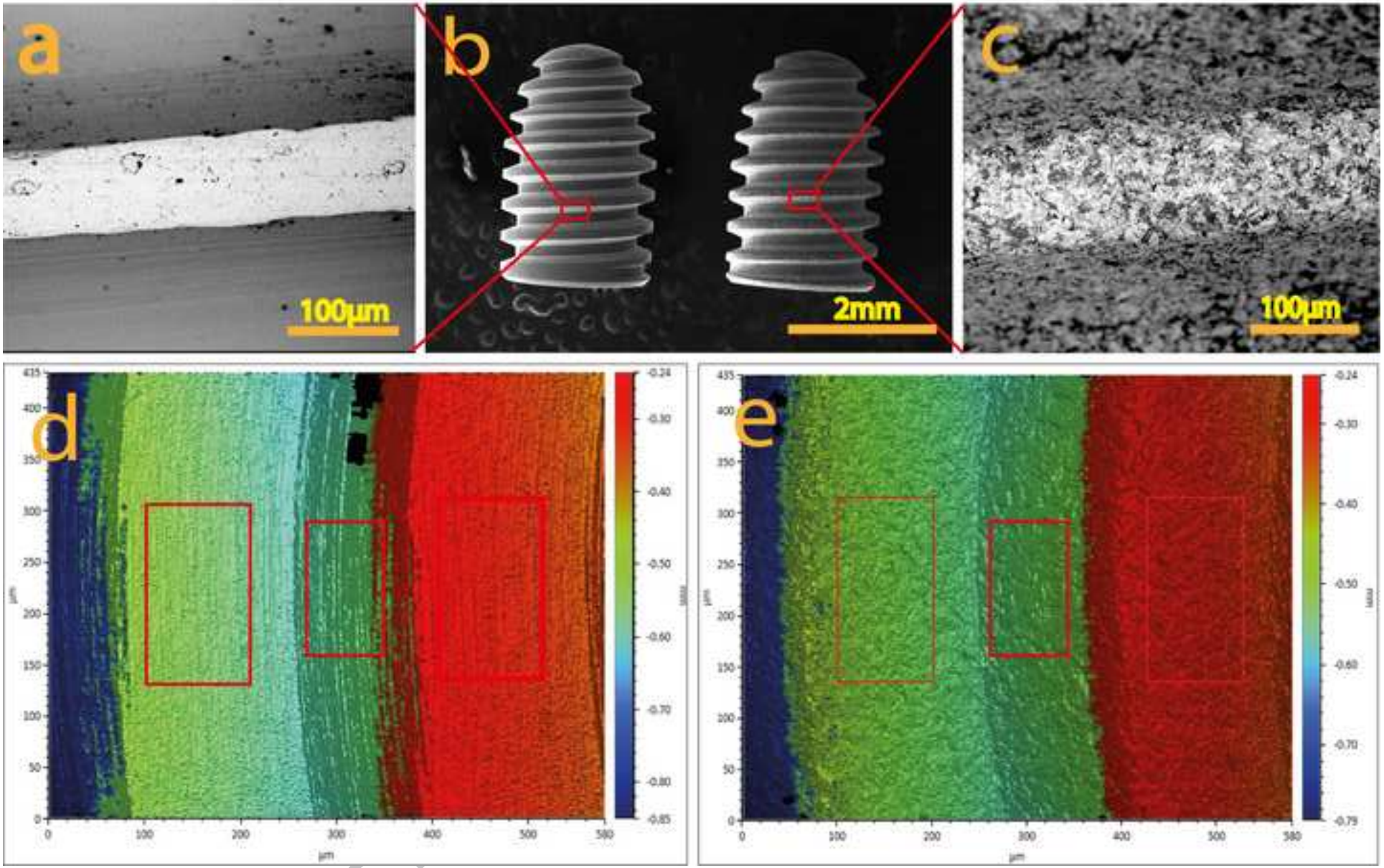

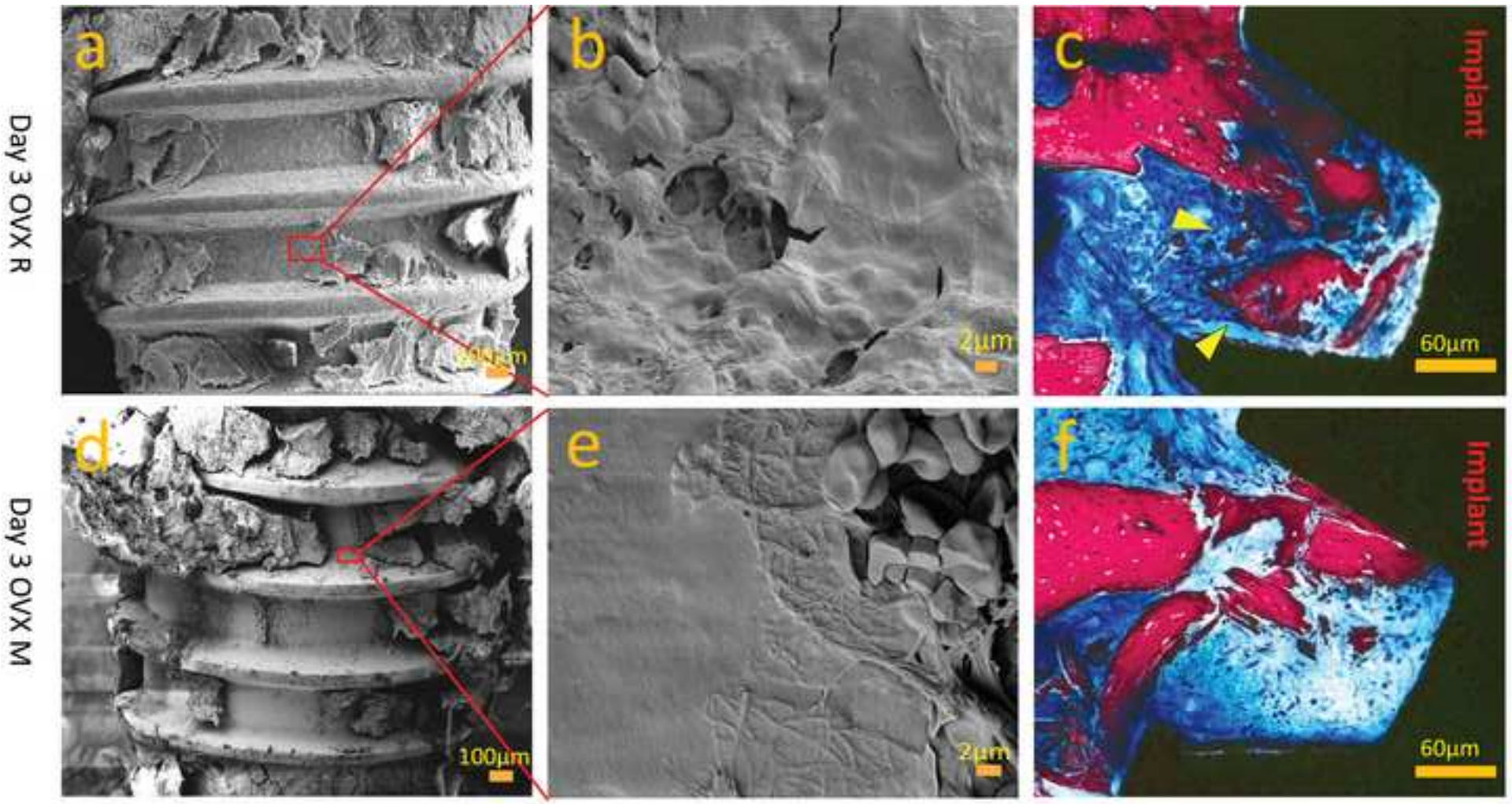

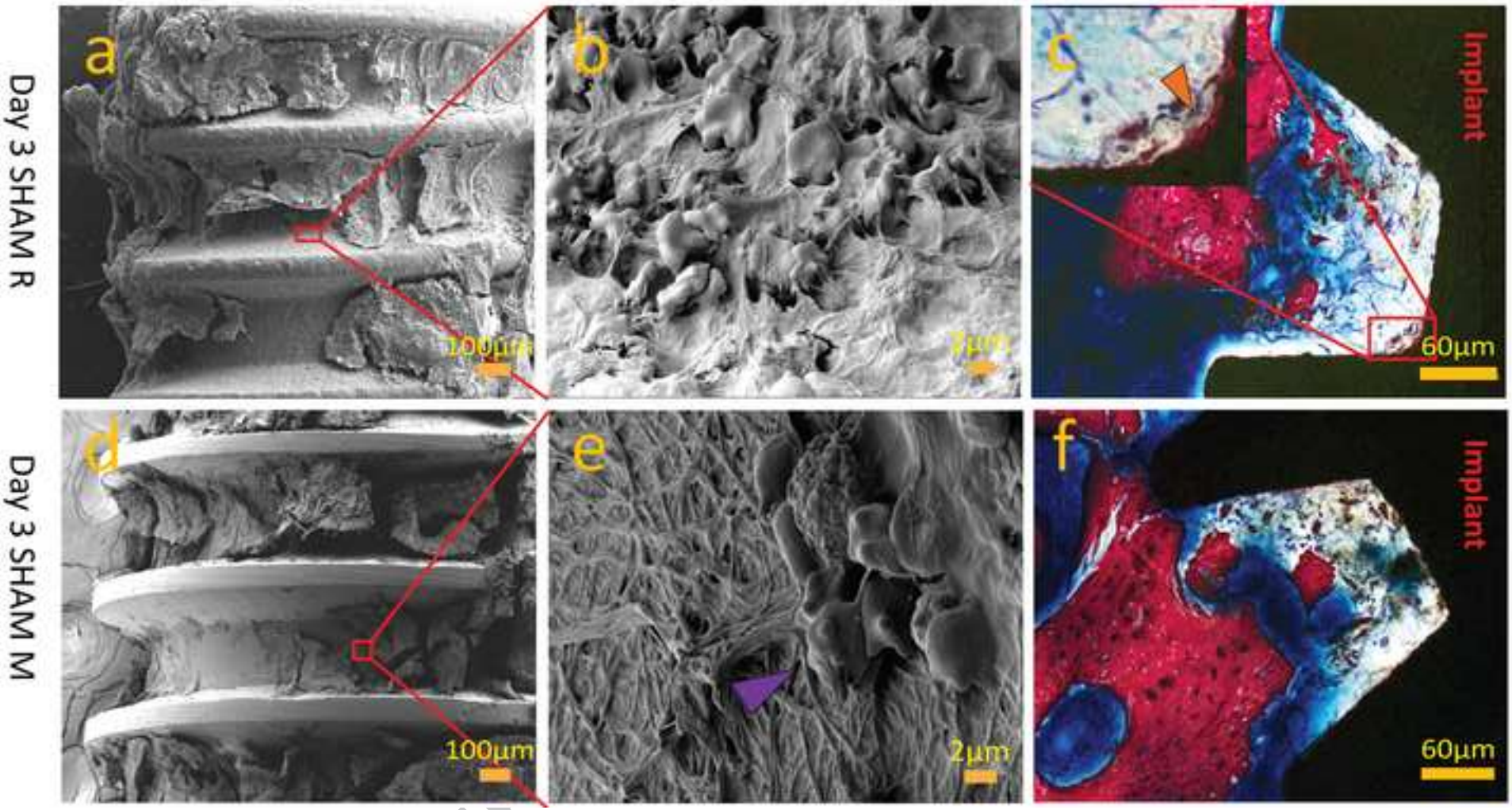

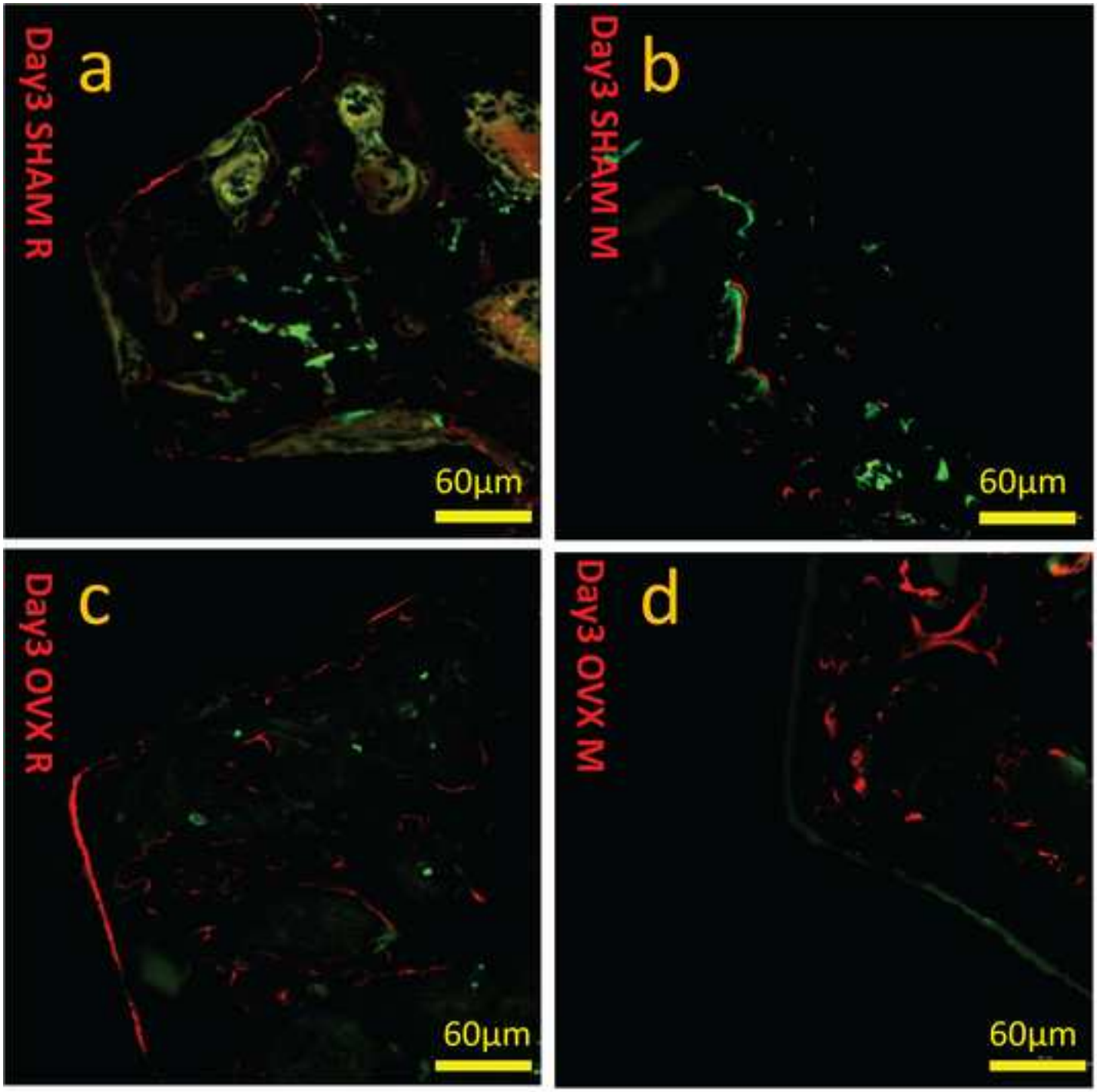

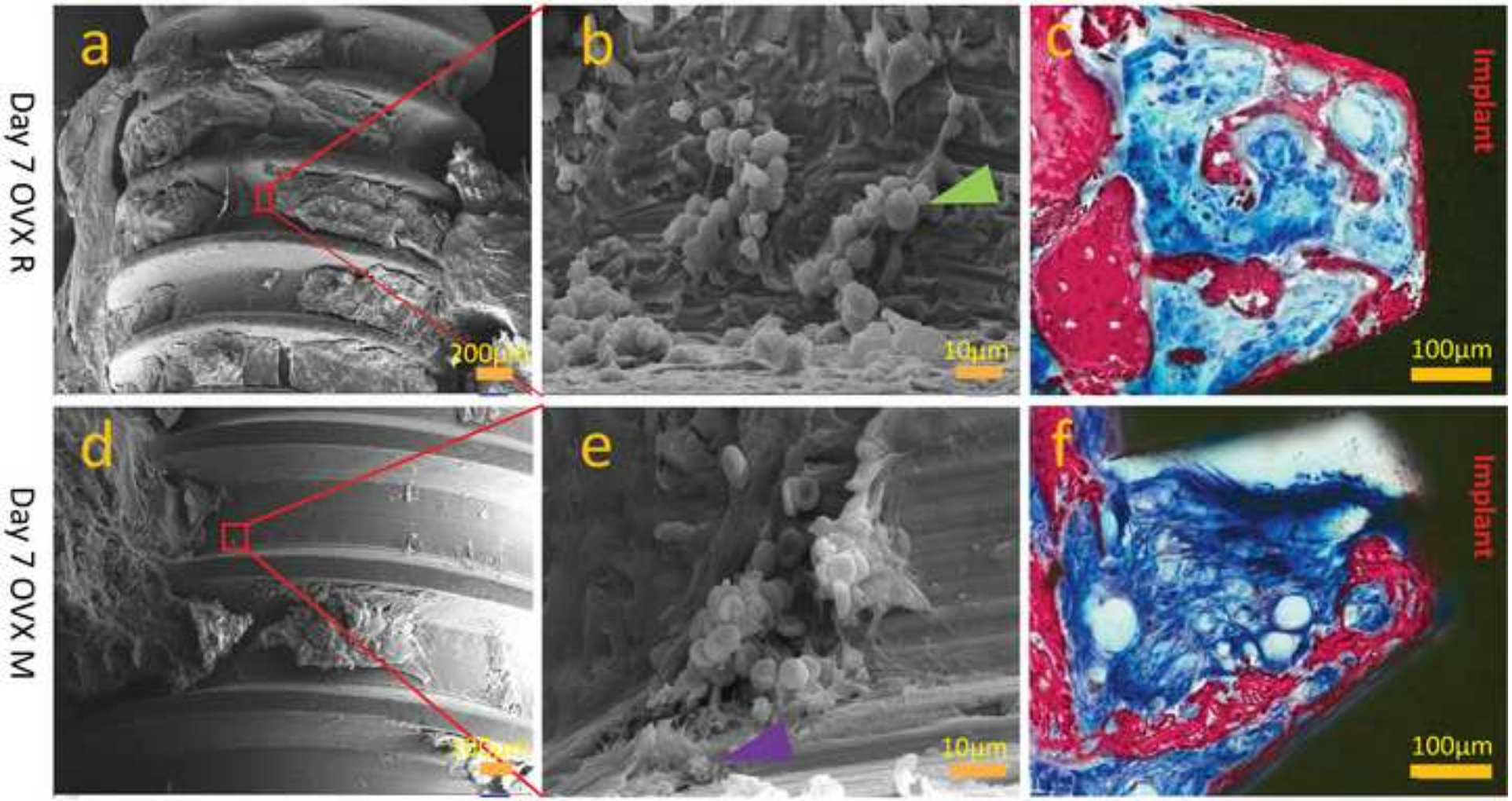

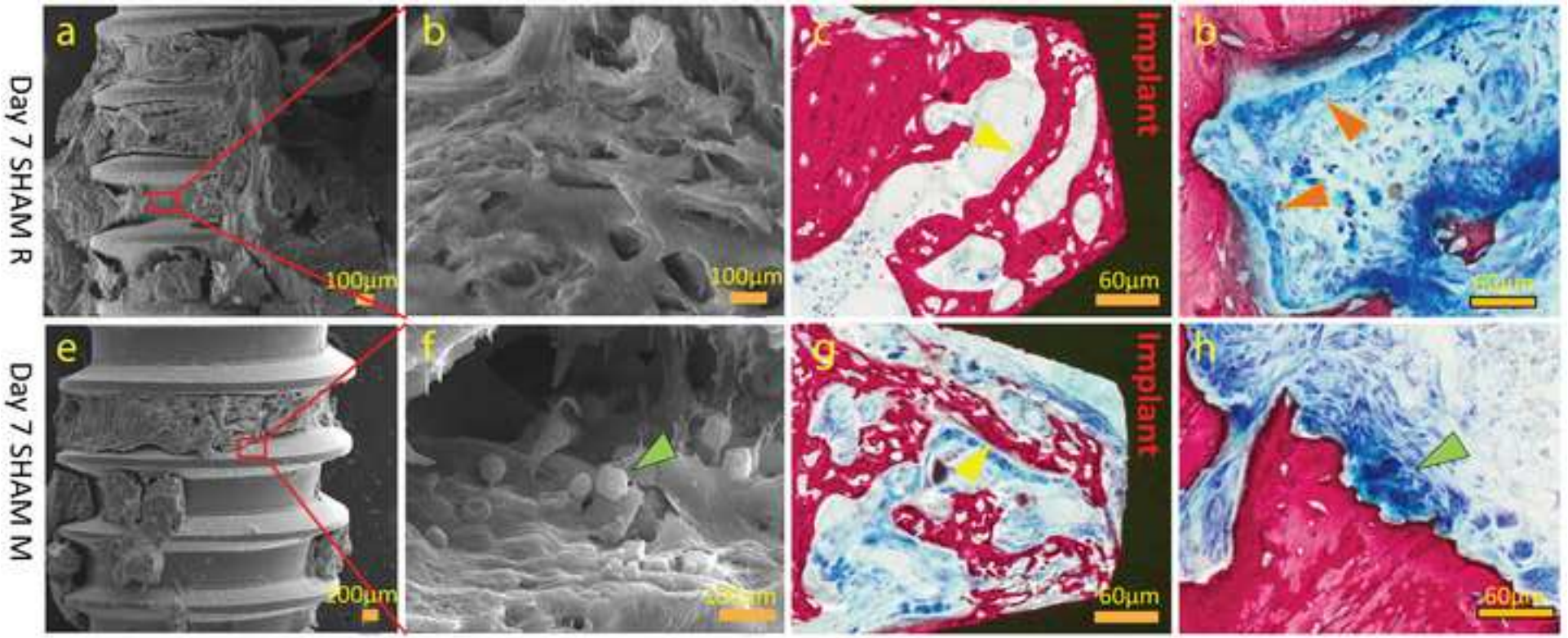

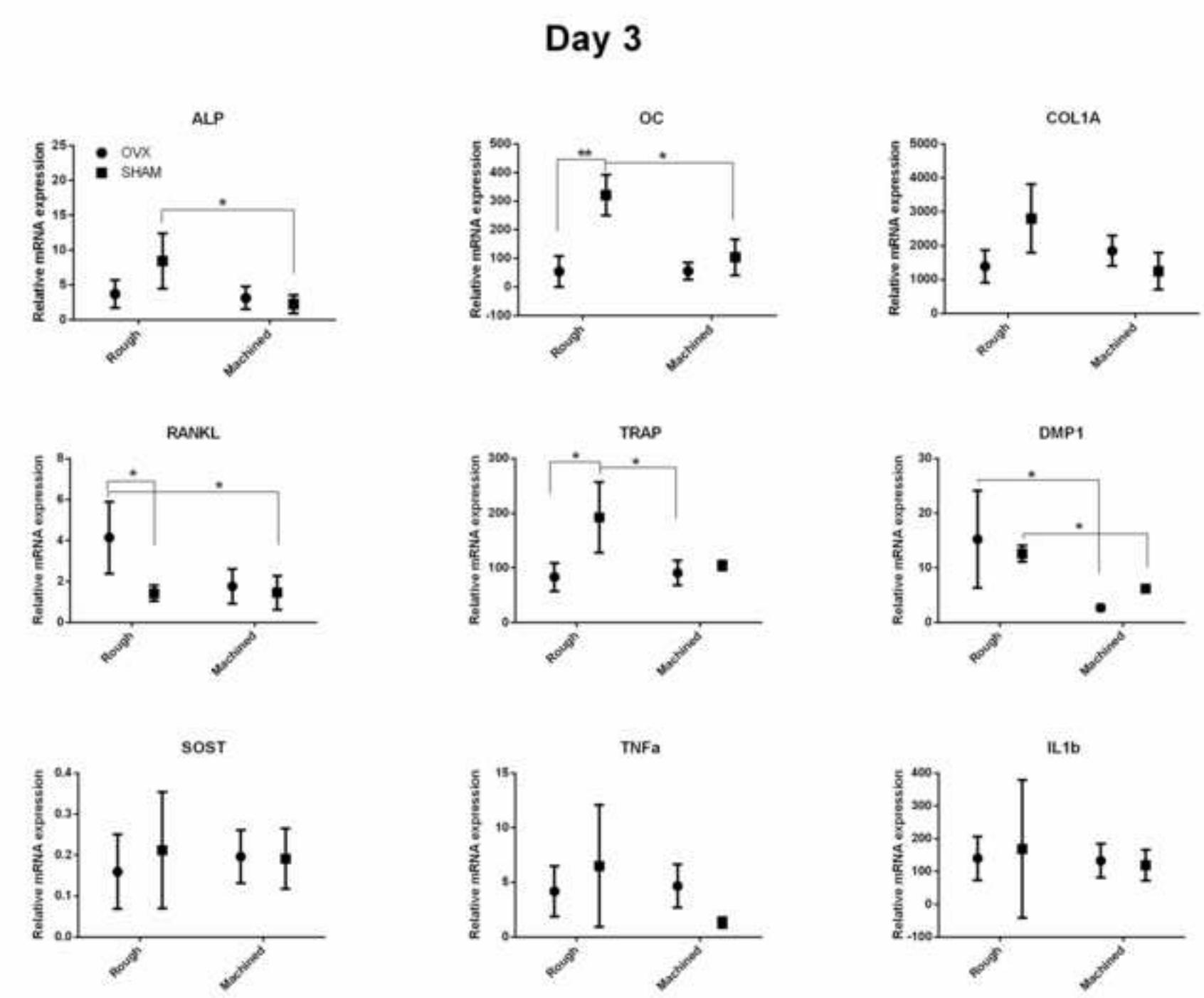

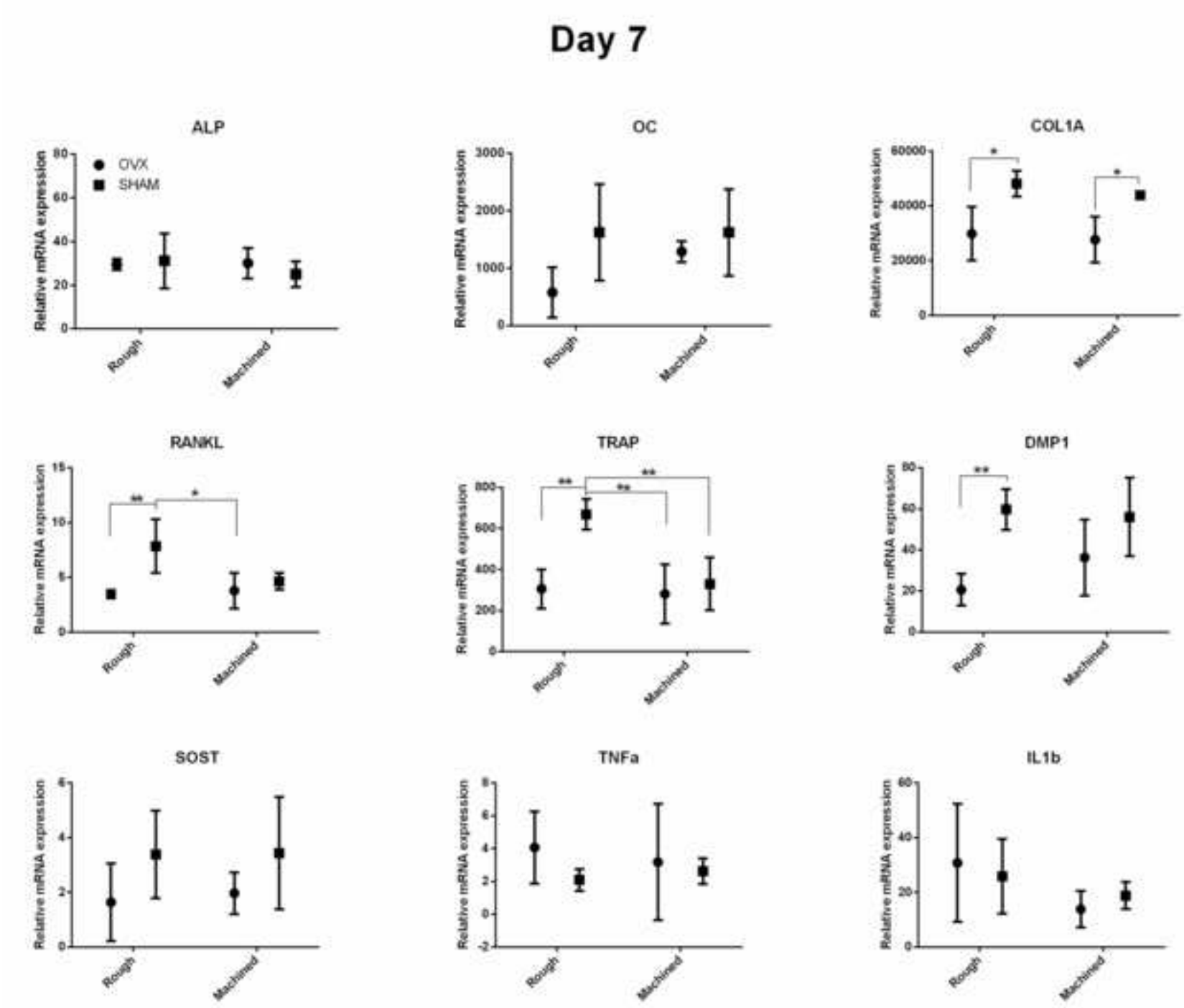

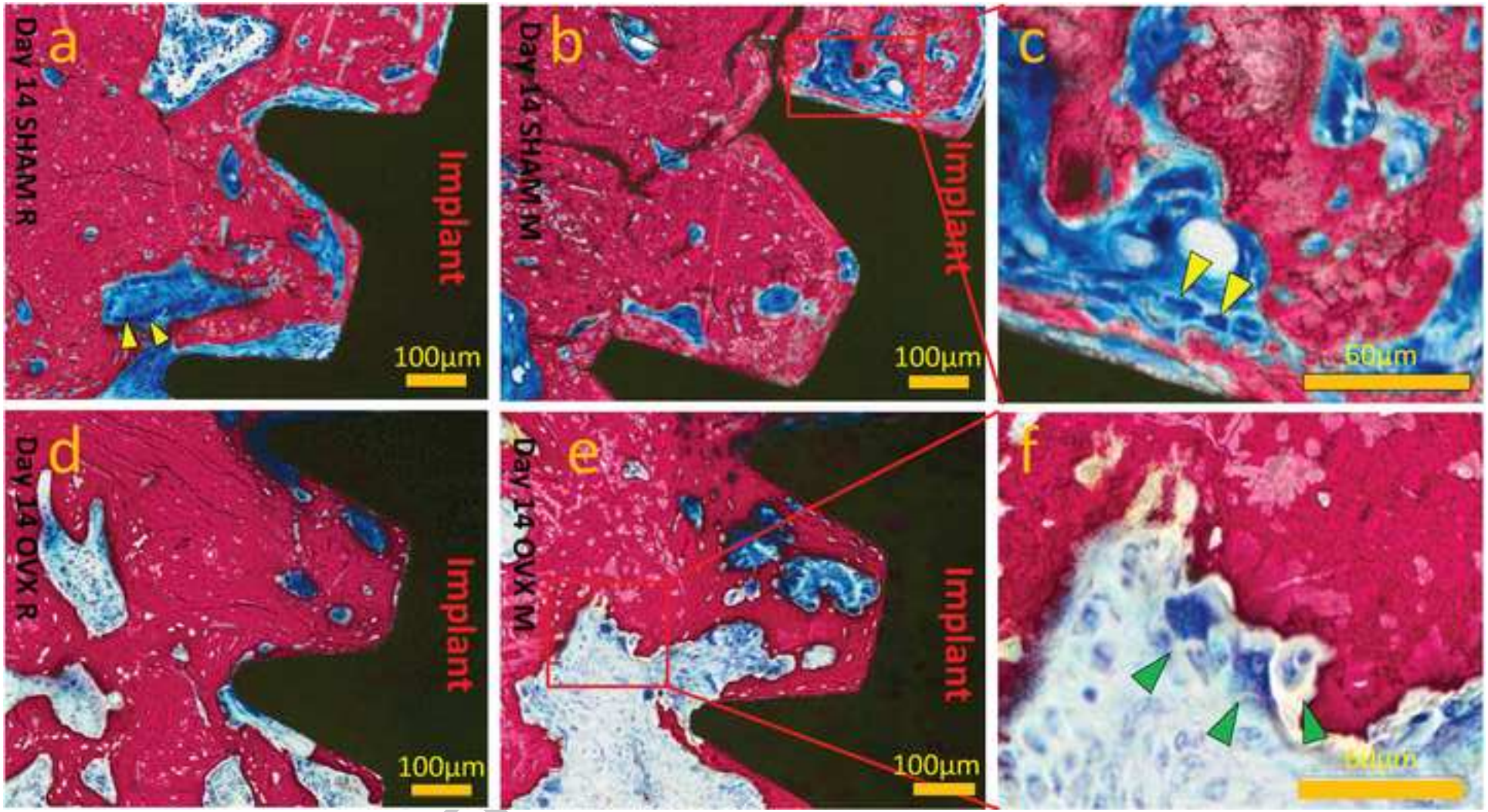

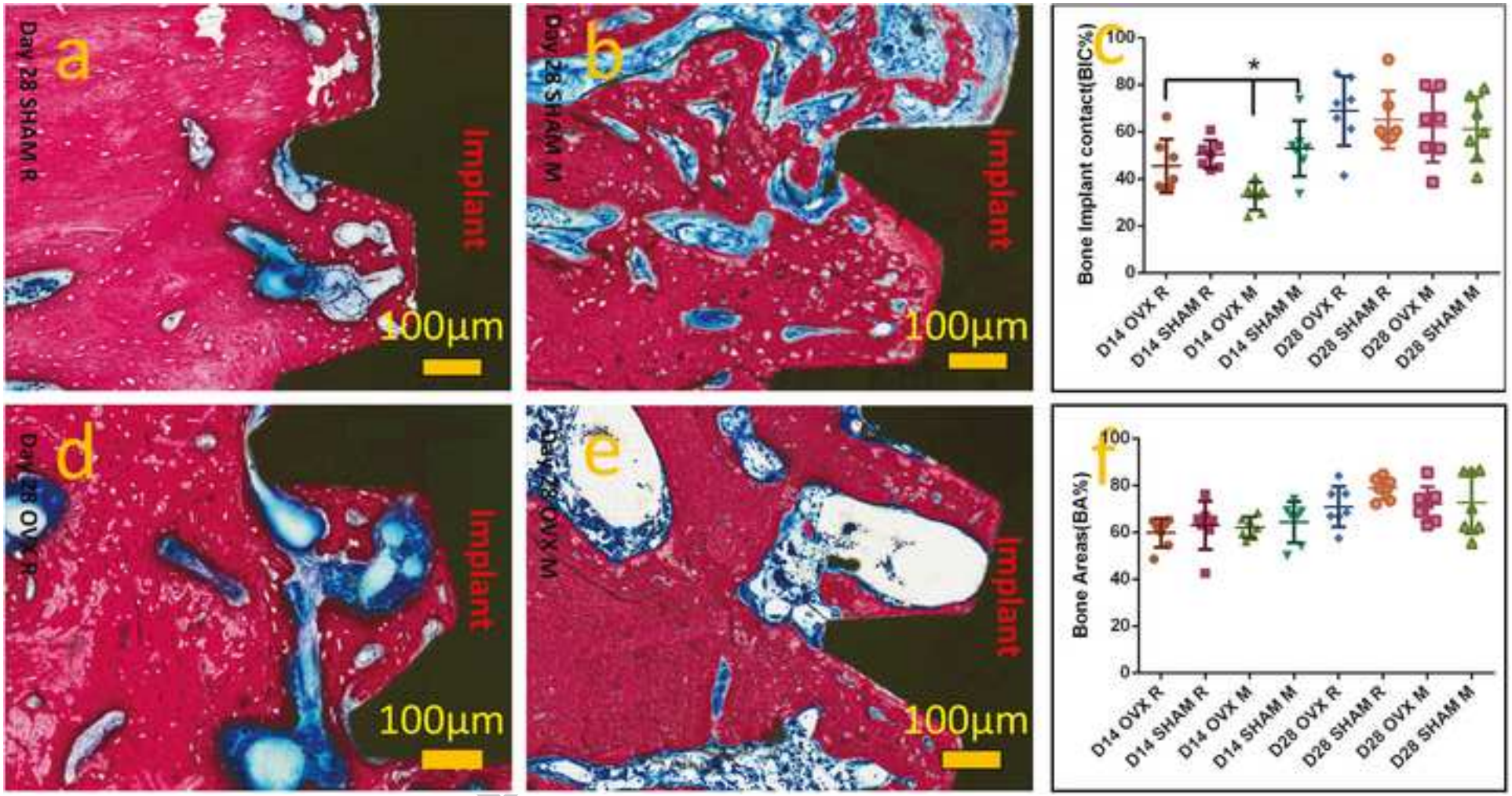

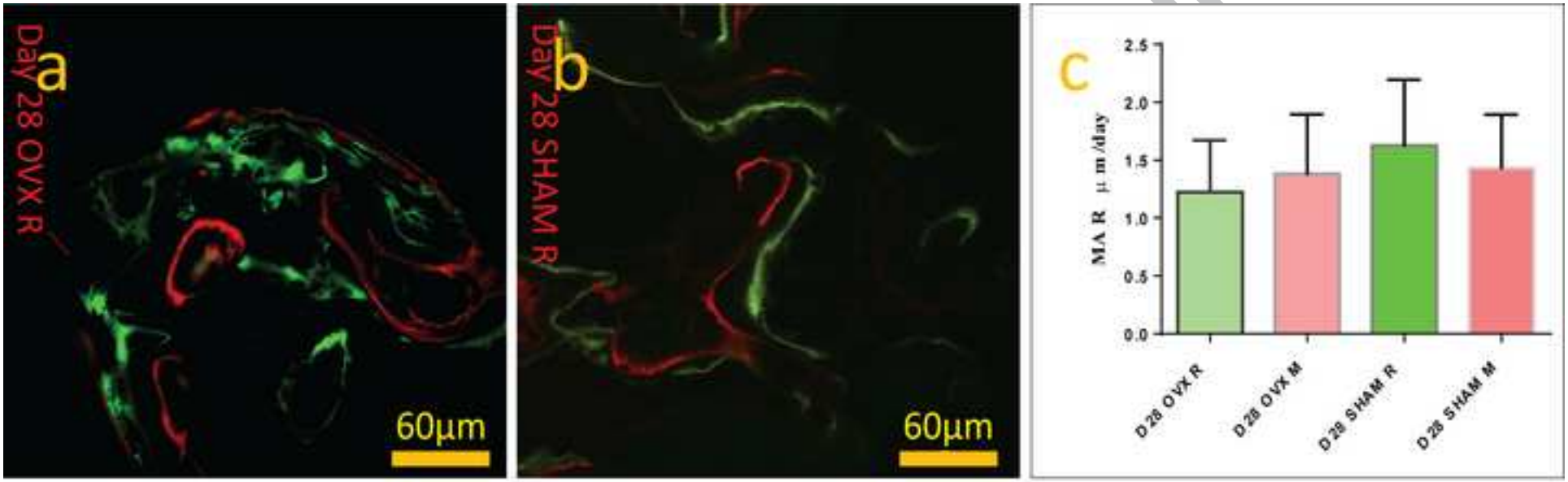

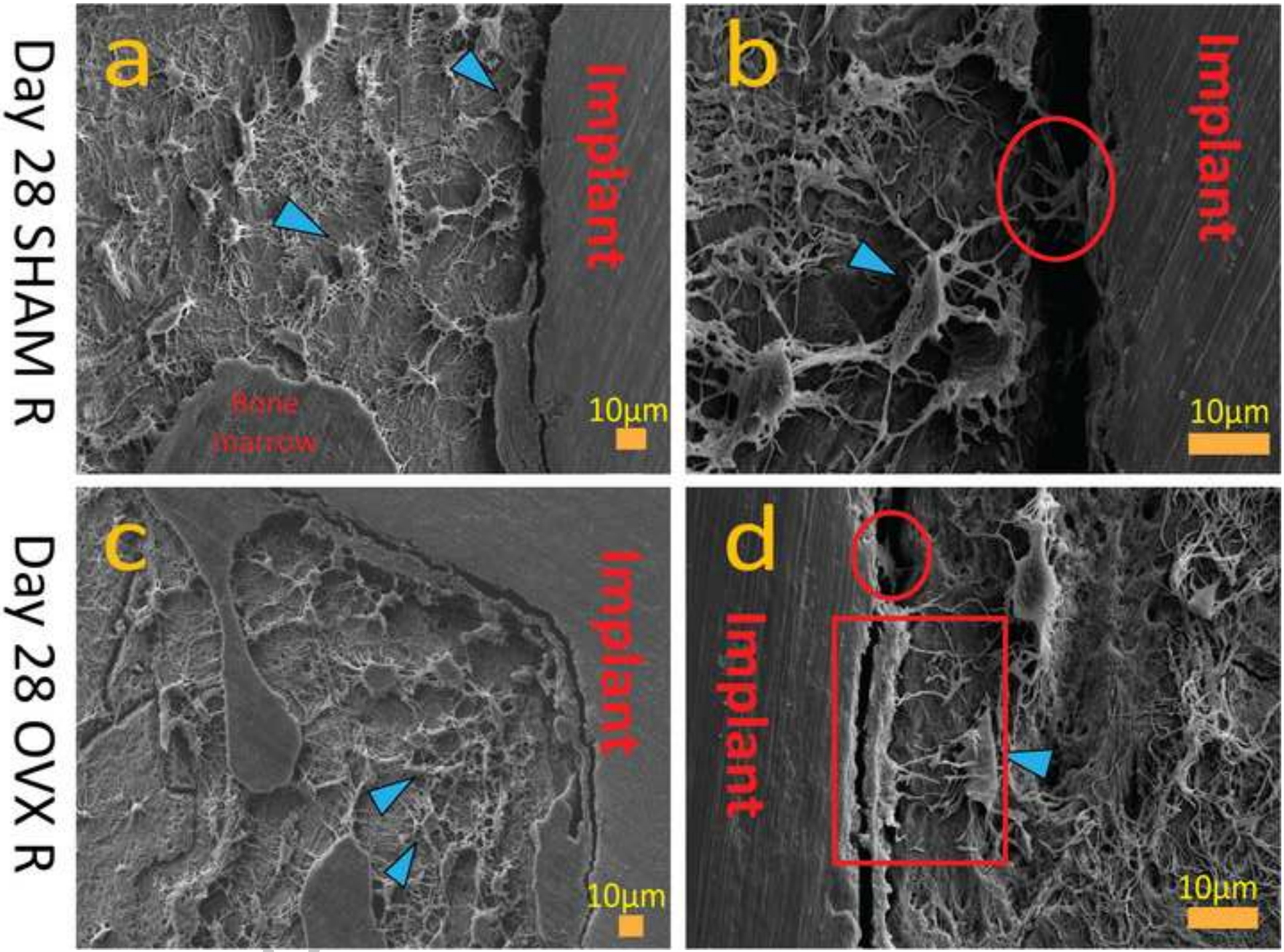

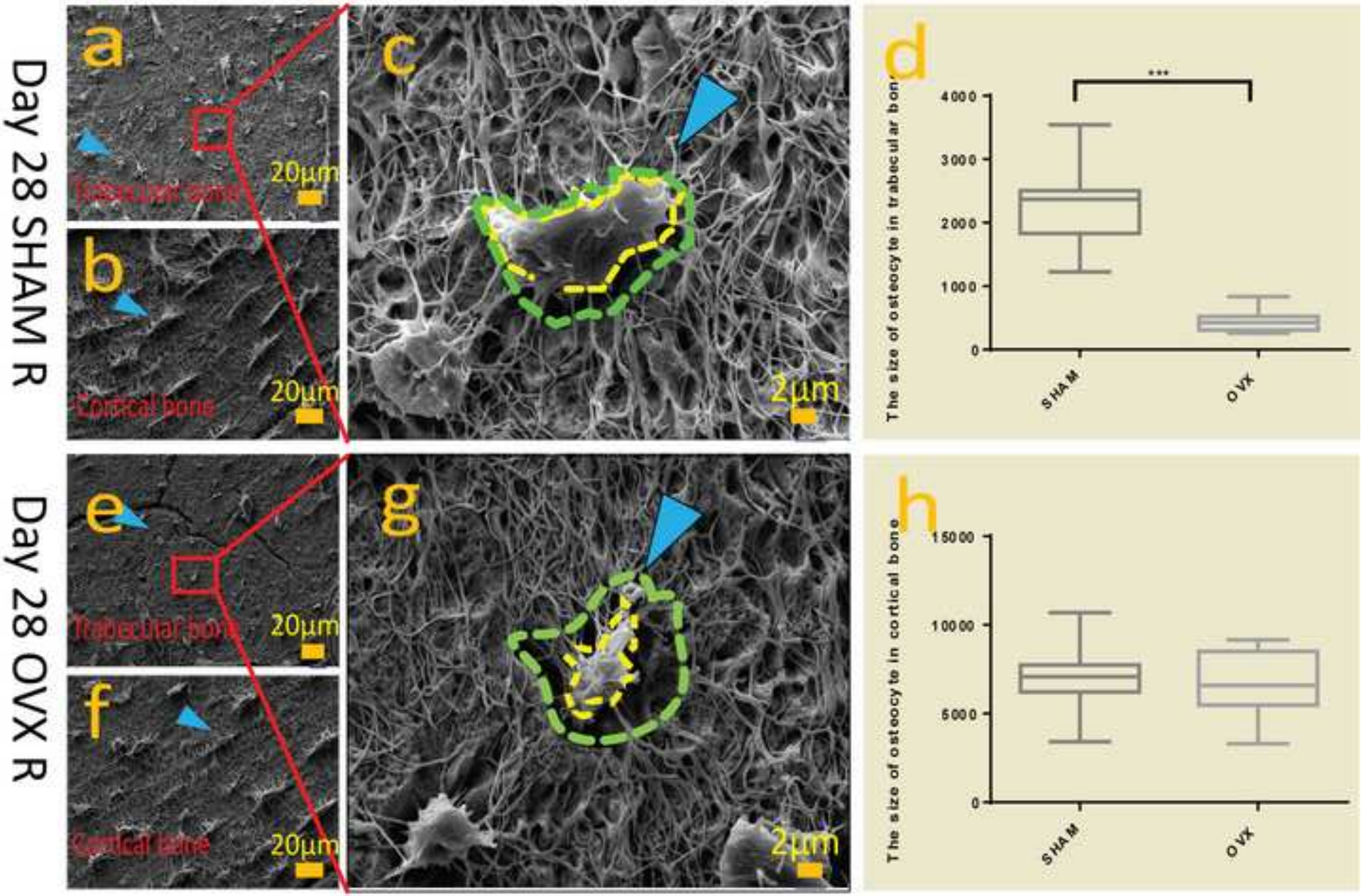

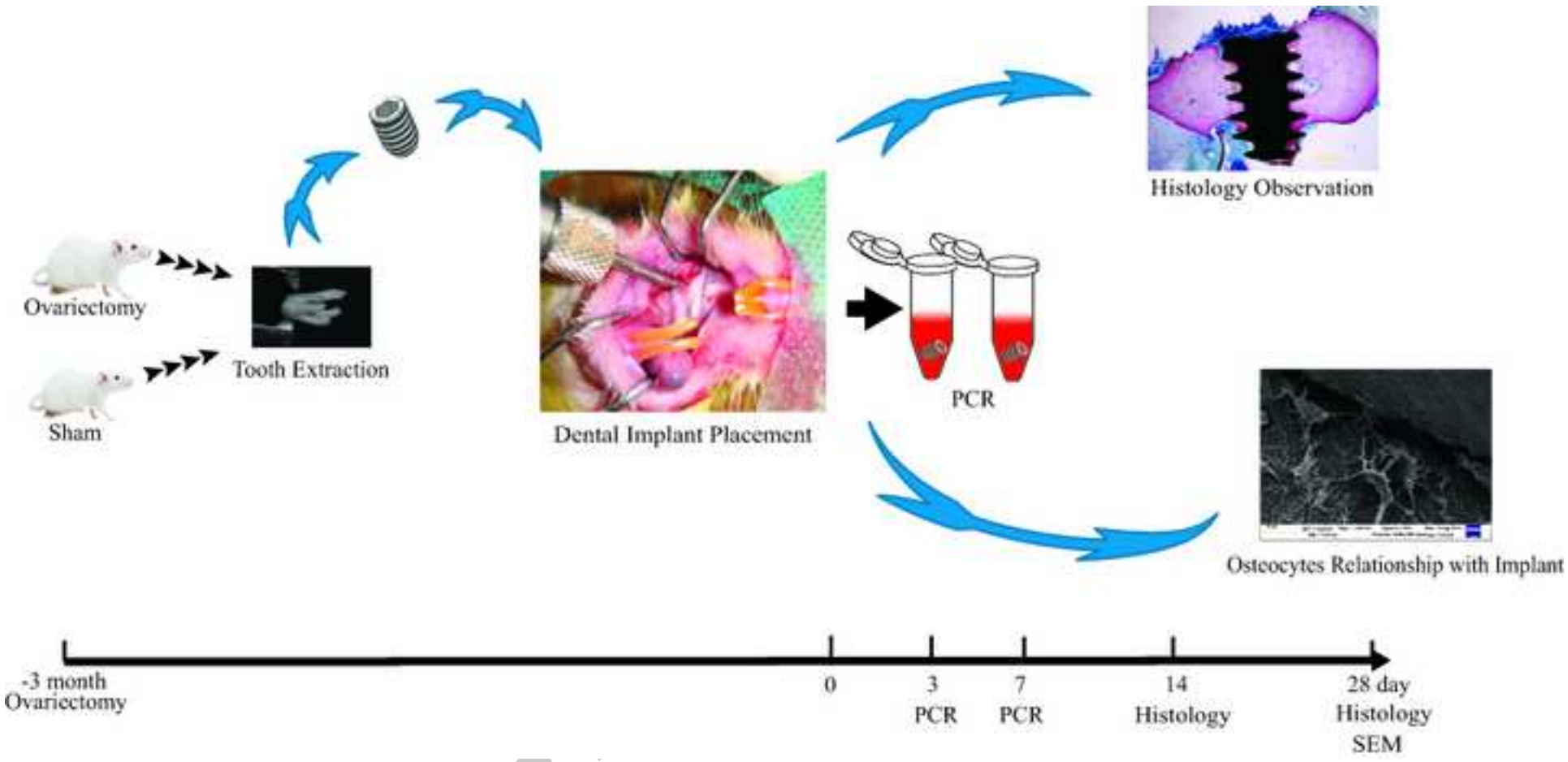

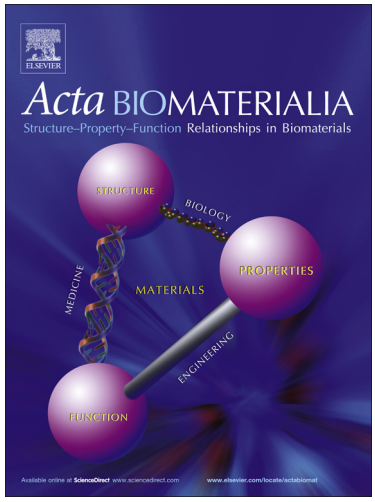

The effects of implant topography on osseointegration under estrogen deficiency induced osteoporotic conditions: histomorphometric, transcriptional and ultra-structural analysis

Zhibin Du, Yin Xiao, Saeed Hashimi, Stephen M. Hamlet, Saso Ivanovski

PII: S1742-7061(16)30312-9
DOI: http://dx.doi.org/10.1016/j.actbio.2016.06.035
Reference: ACTBIO 4307

To appear in: *Acta Biomaterialia*

Received Date: 24 March 2016
Revised Date: 1 June 2016
Accepted Date: 28 June 2016

Please cite this article as: Du, Z., Xiao, Y., Hashimi, S., Hamlet, S.M., Ivanovski, S., The effects of implant topography on osseointegration under estrogen deficiency induced osteoporotic conditions: histomorphometric, transcriptional and ultrastructural analysis, *Acta Biomaterialia* (2016), doi: http://dx.doi.org/10.1016/j.actbio.2016.06.035